Research Square

Preprints are preliminary reports that have not undergone peer review.
They should not be considered conclusive, used to inform clinical practice,
or referenced by the media as validated information.

Lead optimization of novel quinolone chalcone compounds by a structure-activity relationship (SAR) study to increase efficacy and metabolic stability

James Knockleby
Health Sciences North
Aicha Djigo
Health Sciences North
I. Kalhari Lindamulage
Health Sciences North
Chandrabose Karthikeyan
Indira Gandhi National Tribal University
Piyush Trivedi
Bharati Vidyapeeth Deemed University
Hoyun Lee (hlee@hsnri.ca)
Health Sciences North

Research Article

Keywords: CTR compound, anticancer agent, SAR, quinolone, chalcone; breast cancer cell, NCI-60 cancer panel

Posted Date: February 16th, 2021

DOI: https://doi.org/10.21203/rs.3.rs-198850/v1

License: This work is licensed under a Creative Commons Attribution 4.0 International License. Read Full License

Abstract

Many agents targeting the colchicine binding site in tubulin have been developed as potential anticancer agents. However, none has successfully made it to the clinic, due mainly to dose limiting toxicities and the emergence of multi-drug resistance. Chalcones targeting tubulin have been proposed as a safe and effective alternative. To identify the most effective anticancer chalcone compound, we synthesized 17 quinolone-chalcone derivatives based on our previously published CTR-17 and CTR-20, and then carried out a structure-activity relationship study. We identified two compounds, CTR-21 [((E)-8-Methoxy-3-(3-(2-methoxyphenyl)-3-oxoprop-1-enyl) quinolin-2(1H)-one)] and CTR-32 [((E)-3-(3-(2-ethoxyphenyl)-3-oxoprop-1-enyl) quinolin-2(1H)-one)] as potential leads, which contain independent moieties that play a significant role in their enhanced activities. At the nM range, CTR-21 and CTR-32 effectively kill a panel of different cancer cells originated from a variety of different tissues including breast and skin. Both compounds also effectively kill multi-drug resistant cancer cells. Most importantly, CTR-21 and CTR-32 show a very high degree of selectivity against cancer cells. *In silico*, both of them dock near the colchicine-binding site with similar energies. However, only CTR-21 effectively prevents tubulin polymerization, leading to the cell cycle arrest at G2/M and, eventually, cancer cell death by apoptosis. Perhaps not surprisingly, the combination of CTR-21 and ABT-737, a Bcl-2 inhibitor, showed synergistic effect in killing cancer cells, since we previously found the “parental” CTR-20 also exhibited synergism. Taken together, CTR-21 can potentially be a highly effective and relatively safe anti-cancer drug.

Introduction

Microtubules, the polymers of alpha and beta tubulin proteins, are essential for a wide range of cellular functions including proliferation, intracellular trafficking, cell signaling, cell shape and migration, and even tumor angiogenesis. Drugs targeting microtubules have been shown effective, with their potency even exceeding their anti-mitotic properties[1,2]. Microtubule-targeting agents (MTAs) have thus been widely used as chemotherapeutics for several decades and remain relevant in cancer therapy today, either administrated alone or in combination with other regimens. From colchicine, one of the oldest drugs, to more recent drugs such as paclitaxel and its analogues, MTAs interact with tubulin at different sites and through different mechanisms of actions (MOA)[3]. Microtubule targeting drugs are classified in two major groups: microtubule-stabilizing agents which promote microtubule polymerization while also inhibiting disassembly by binding to the tubulin polymer, and microtubule-destabilizing agents which bind to the tubulin dimers and block microtubule polymerization[3,4]. Although these drugs have been on the market for decades, they suffer from some common drawbacks that limit their effectiveness in many cases. These include acquired drug resistance and dose-limiting toxicities. The latter, in particular, prevents colchicine from being deployed as a cancer therapeutic[5,6].

Our interest in finding novel safe and effective anticancer agents has focused on refining natural product compounds into lead candidates. One family of compounds that has shown great interest over the past few decades are chalcones. Chalcones are found in flavonoids in many different edible plants as secondary metabolites[7]. Chalcones contain a three carbon α, β unsaturated carbonyl core that links two phenyl rings. The phenyl rings offer sites of modification with a diversity of single and multiple additions in order to maximize effectiveness, increase stability, and enhance solubility and other chemical properties. Chalcones that contain similar trimethoxyphenyl rings as colchicine show promise as anti-proliferative agents[8,9], suggesting that methyoxy groups are likely important modifications for structure-activity studies.

Due to their simple chemistry which allows for an abundance of substitutions coupled with their known anti-proliferative activities, we synthesized 19 chalcone derivatives using the Claisen-Schimdt condensation. The quinolone chalcone compounds (named CTRs) microtubule-destabilizing agents, two of which (CTR-17 and CTR-20) showed a selective and potent anti-tubulin activity and caused a prolonged mitotic arrest at the spindle assembly checkpoint (SAC), eventually lead to cell death[10]. We sought to enhance their anti-growth/proliferation properties with a structure–activity relationship (SAR) approach to design and synthetize more effective candidates that would be more potent against cancer cells while sparing normal cells at low concentrations and maintaining selectivity. We identified that CTR-21 [((E)-8-Methoxy-3-(3-(2-methoxyphenyl)-3-oxoprop-1-enyl) quinolin-2(1H)-one)] is the most desirable anticancer agent among this series of chalcone compounds.

Results

Chemistry. The synthesis of the 19 quinolone chalcones were carried out using acetanilides commercially available or synthesized using standard protocols from anilines[11] (Fig. 1). 2-chloroquinoline 3-carboxaldehydes were synthesized by treating acetanilides with DMF and $POCl_3$ under Vilsmeier Haack conditions[12]. We then synthesized 3-(2-chloroquinolin-3-yl)-1-phenylprop-2-en-1-ones utilizing Claisen-Schmidt condensation of the 2-chloroquinoline-3-carbaldehydes under basic conditions (sodium methoxide or NaOH) with the appropriate acetophenones[13,14] The 3-(2-chloroquinolin-3-yl)-1-phenylprop-2-en-1-ones were refluxed with aqueous glacial acetic acid to induce O-nucleophilic substitution at the 2-chloro group of the quinoline ring to derive the corresponding quinolone chalcones. Compounds were confirmed with a combination of their infrared (IR) spectroscopic ^1H NMR and mass spectral data (see Methods).

CTR-21 and CTR-32 are the most effective anti-proliferative quinolone chalcones examined. We had initially determined that quinolone chalcones were promising anti-proliferative through a first round screening and identified CTR-17 and CTR-20 as favorable structures for anticancer activity[10]. CTR-17 and CTR-20 have been modelled to bind to the colchicine binding pocket on β–tubulin and cause a prolonged mitotic arrest at the spindle assembly checkpoint, eventually leading to apoptosis. We carried out a comparative SAR study to determine if we could further optimize the quinolone chalcone to maximize efficacy. The Sulforhodamine B (SRB) assay was used to measure the anti-proliferative/cell killing activities of CTRs, for which several different cell lines were use: the cervical cancer HeLa, the breast cancer cell lines MDA-MB231, MDA-MB468, MDA-MB231TaxR (an induced paclitaxel-resistant sub-cell line of the MDA-MB231[10]) and MCF7. In addition, a subset was tested against the melanoma cell lines MZ-MEL-3.1, Mel-SOE, UKRV-Mel-38, UKRV-Mel-17 and MDA-MB-435 (Table 1, Supplemental Table S1). CTR-21 and CTR-32 were highly potent with GI_{50} ranging from 5 nM to 91 nM. Notably, the ability for CTR-21 and CTR-32 to maintain effectiveness against MDA-MB231TaxR suggests that these two compounds remain refractive to multi-drug resistance mechanisms, as previously shown by CTR-20[10]. CTR-21 and CTR-32 were also highly effective against the NCI-60 panel of representative cancer cell lines (Supplemental Figs. S1-S8).

Table 1
GI_{50} values of quinolone chalcone analogs on breast cancer, melanoma and cervical cancer cells.*

	Melanoma cell lines				Breast cancer cell lines					Cervical cancer
	MZ-Mel-3	Mel-SOE	UKRV-Mel-38	UKRV-Mel-17	MDA-MB435	MDA-MB231	MDA-MB231-TaxR	MDA-MB468	MCF7	HeLa
CTR17 (nM)	227 ± 30	786 ± 52	626 ± 154	504 ± 33	290 ± 66	657 ± 72	1,299 ± 83	320 ± 26	485 ± 97	280 ± 78
CTR18 (nM)	239 ± 13	817 ± 34	746 ± 177	596 ± 162	307 ± 7	530 ± 119	1,214 ± 179	304 ± 2	510 ± 38	443 ± 112
CTR19 (nM)	6,832 ± 957	10,095 ± 64	3,766 ± 206	11,166 ± 1,660	4,723 ± 2,761	6,506 ± 1,388	7,089 ± 1,059	3,538 ± 60	11,910 ± 564	6,823 ± 1,389
CTR20 (nM)	98 ± 21	338 ± 78	338 ± 33	283 ± 57	90 ± 10	216 ± 21	966 ± 163	408 ± 12	194 ± 21	124 ± 36
CTR21 (nM)	6 ± 1	27 ± 5	13 ± 3	9 ± 2	7 ± 2	17 ± 3	32 ± 8	29 ± 10	16 ± 5	8 ± 3
CTR32 (nM)	6 ± 2	33 ± 9	22 ± 3	18 ± 3	13 ± 5	20 ± 2	22 ± 4	26 ± 0	27 ± 6	11 ± 2
CTR40 (nM)	11 ± 0	53 ± 4	42 ± 11	28 ± 5	23 ± 0	30 ± 4	54 ± 13	77 ± 13	41 ± 5	19 ± 1
Tax (nM)§	58 ± 15	60 ± 16	6 ± 1	14 ± 4	4 ± 1	3 ± 1	131 ± 35	9 ± 3	6 ± 1	8 ± 1
Noco (nM)§	23 ± 2	51 ± 11	34 ± 3	39 ± 1	18 ± 2	35 ± 4	47 ± 11	48 ± 7	33 ± 7	25 ± 1

* GI_{50} values were derived from a non-linear sigmoidal dose-response (variable slope) curve fitted by GraphPad Prism v.4.03 software.

§Tax and Noco denote paclitaxel and Nocodazole, respectively.

SAR analysis reveals two separate moieties that synergistically increase anti-growth/proliferative effects. The diversity of chemical groups in our library allowed us to determine which moieties found on the two ring structure might best enhance cytotoxicity (Fig. 1). CTR-17 shows the simplest design with an unsubstituted quinolone ring linked to 2-methoxy phenyl moiety through an 'enone' group and it displays an anti-proliferative activity in the medium range (GI_{50} = 464 nM; Table 1). The 2-methoxy group on the phenyl ring is critically important to the efficacy of the CTRs[15,16]. Introducing a 6-methyl group on the quinolone ring does not lead to any change in efficacy (CTR-18, GI_{50} = 499 nM; Fig. 1) with all 9 cell lines showing similar GI_{50} to that of CTR-17. The introduction of a 5-methoxy to CTR-17 (i.e., CTR-26) does not seem to have an effect either in terms of anti-growth/proliferative activity (GI_{50} = 443 nM), whereas CTR-29 (5-fluorophenyl) has a lower GI_{50} of 118 nM. In contrast, the addition of a 6-methoxy group on the phenyl ring (CTR-25, GI_{50} = 1.6 μM, Supplemental Table 1) leads to a 4-fold increase in GI_{50}. This suggests the possibility that the presence of a second methoxy group may induce steric hindrance or adverse interactions if a methoxy group is near the quinolone group. In contrast, a single methoxy group on the phenyl ring

may not hinder the quinolone group, as the phenyl ring can rotate on the axis on its bond with the carbonyl of the enone group which may affect how the CTR binds to its target.

Examining the SAR of the methoxy group placement on the quinolone ring, we determined that if there is a methoxy group present, its position is vitally important to the cytotoxic activity of the compound. CTR-19, which has a 7-methoxy on the quinolone ring is the least effective analog out of the CTRs in terms of anti-proliferative activity with an average GI_{50} of 7.3 μM (Table 1), whereas the average GI_{50} of CTR-20 (6-methoxy) is 232 nM (Table 1) and CTR-21 (8-methoxy) is 16.4nM (Table 1). The enhanced activity of CTR-20 is likely due to the presence of the methoxy on the C-6 since it is the only difference (i.e., methyl *vs* methoxy) from CTR-18 which shows much lower activity (Table 1). The activity of CTR-24 (6,7-dimethoxy quinolone) is between those of the 6-isomer and the 7-isomer (1.5 μM), which along with the lower toxicity potency of CTR-19 and CTR-23 (compared to CTR-17) suggesting that the 7- position should remain free for maximum efficacy, and that the 8-position is more favorable for cytotoxic activity than the 6-position.

The introduction of a 5-fluoro on CTR-20 (i.e., CTR-37) does not affect its activity contrary to what we observed between CTR-17 and CTR-29. However, when the fluorine group is added on the 4th carbon (i.e., CTR-38), the average value of the GI_{50} drops to 98 nM which - while not making it as potent as CTR-21 – still makes it one of the most active compounds. The addition of a methoxy group has differential effect on the potency of CTR-20 as well, depending on the position, as indicated by CTR-33 (6-methoxy, GI_{50} = 1.1 μM), CTR-34 (5-methoxy, GI_{50} = 648 nM), CTR-35 (4-methoxy, GI_{50} = 2 μM), and CTR-36 (4-trifluoromethoxy, GI_{50} = 805 nM). This evidence suggests that, although the 2-methoxy group on the phenyl ring is important for activity, we can enhance the activity of the compound by adding may impede activity.

Finally, substituting the 2-methoxyphenyl group for a 2-ethoxyphenyl improved the activity of the compounds. Indeed CTR-32 which, similarly to CTR-17, possesses no additional group on the quinolone but has a 2-ethoxy group on the phenyl ring (Fig. 1) displays one of the lowest average GI_{50} values of the entire collection (20 nM; Table 1). Furthermore, another compound with a 2-ethoxygroup on the phenyl ring (in combination with a 6-methoxy on the quinolone ring), CTR-40 exhibited the third strongest activity (GI_{50} = 36 nM; Table 1). It is highly notable that replacing the 2-methoxy group of the phenyl group (CTR-17) by a 2-ethoxy group (CTR-32; Table 1) resulted in a 23-fold decrease in GI_{50}. It is also highly notable that introducing an 8-methoxy on the quinolone group (CTR-21; Table 1) with keeping the 2-methoxyphenyl renders a 31-fold decrease. One concern of enhancing the activity of the CTR compounds is that toxicity is increased towards non-malignant cells. We previously showed that CTR-17 and CTR-20 are selective against malignant when compared their efficacies against non-malignant cells. Therefore, we next sought to determine the cytotoxicity of the most promising CTR compounds against primary melanocytes and peripheral blood mononuclear cells (PBMCs). We found that CTR-21 and CTR-32 are far less cytotoxic toward primary cells compared to cancer cell lines (Table 2). Comparing the selectivity index (SI) of the primary melanocytes versus the average GI_{50} of cancer cells, both CTR-21 and 32 have similar SIs (CTR-21: 157 fold; CTR-32: 158 fold; Table 2). There is a slightly smaller SI between cancer cells and PBMCs (CTR-21: 106 fold; CTR-32: 67 fold; Table 2), but still a substantial difference between normal and cancer cells. Taken together, these data indicate that we have identified two independent moieties on the CTR backbone that can enhance activity without sacrificing selectivity.

Table 2
GI_{50} values of quinolone chalcone analogs on primary skin and blood cells.*

	Primary skin cells			PBMC§		
GI_{50}	Melanocytes #1	Melanocytes #2	Selectivity Index	PBMC #1	PBMC #2	Selectivity Index
CTR-21 (nM)	2,092 ± 804	3,052 ± 960	157	1,857 ± 336	1,632 ± 317	106
CTR-32 (nM)	2,631 ± 782	3,627 ± 1083	158	1,881 ± 147	787 ± 396	67
* GI_{50} values were derived from a non-linear sigmoidal dose-response (variable slope) curve fitted						
by GraphPad Prism v.4.03 software. § PBMC denotes peripheral blood mononuclear cells						

CTR 21 reduces the steady state of microtubule polymerization by binding to β-tubulin. We previously found that CTR-17 and CTR-20 inhibited microtubule polymerization as they competed with colchicine for binding to the colchicine-binding site[10]. Consistent with the notion that the CTRs play a role in disrupting microtubule dynamics, we next determined if the enhancement of efficacy seen in CTR-21 and CTR-32 were due to the disruption of microtubule dynamics in an *in vitro* tubulin polymerization assay (Fig. 2a). Compared to the control, the paclitaxel curve has a shorter nucleation phase, steeper growth phase, and reaches steady state quicker, as would be seen with a microtubule stabilizer. Nocodazole has a slightly lower V_{max} compared to the control (Supplemental Fig. S9) and a reduced steady-state acting as a microtubule destabilizer. Under these conditions, CTR-21 has a similar V_{max} to the control (Supplemental Fig. S9) yet a reduced steady-state, indicating that it is a tubulin destabilizer. CTR-32, however, does not affect the steady state dynamics or V_{max} of tubulin polymerization. Therefore, even though CTR-32 arrests the cells in G_2/M (Supplemental Fig. S10), it does not appear to affect microtubule polymerization dynamics by directly interacting with α or β tubulin.

We previously showed through *in vitro* studies and *in silico* modeling that CTR-17 and CTR-20 bind to tubulin overlapping the colchicine binding site, and inhibit tubulin polymerization[10]. Since there was a marked difference between the efficacy of CTR-20 compared to CTR-21 and CTR-32, we first sought to model the potential binding of these compounds in relation with each other. We found that the binding of CTR-21 and CTR-32 to the colchicine binding pocket did not have a notable difference in free energy when compared to CTR-20 or other CTRs (Fig. 2b), suggesting that the modifications did not adversely affect tubulin binding in general. However, the residues interacting with CTR-21 are different than the ones that interact with CTR-20 (Fig. 2c). CTR-21 potentially interacts with Pro175 (of β-tubulin), a part of the vinblastine binding site[17] through hydrogen bonding with the quinolone ring nitrogen and also interacts with Thr179 (of α-tubulin) a part of the colchicine binding pocket, through hydrogen bonding with the carbonyl group on the quinolone ring. CTR-20 also interacts with a part of the colchicine-binding pocket, but the only hydrogen bonding occurs on β-tubulin residues, both between the quinolone methoxy group and the Cys241 residue on β-tubulin, and the quinolone nitrogen on Asp251 of β-tubulin. These *in silico* docking data suggest that CTR-21 acts in essence as a hybrid of two microtubule interacting drugs in an overlapping pocket (colchicine and vinblastine), between the two subunits of the tubulin dimer. Furthermore, the differences between the methoxy groups on CTR-20 and CTR-21 are evident when compared with colchicine in three-dimensional space (Fig. 2d). CTR-21 interacts in a perpendicular manner at the opposite end of the colchicine binding site when

compared to CTR-20 (Fig. 2d). The carbonyls of both CTR-21 and colchicine form hydrogen bonds with the amino nitrogen of Thr179 in α-tubulin. Additionally, both compounds interact with Ala180 in a hydrophobic manner, CTR with the 2-methoxy phenyl group and colchicine with the acetamide group. However, the trimethoxy ring on colchicine points in a different direction compared to CTR-21 quinolone group, which interacts with Pro175 of the vinblastine-binding site rather than further in the colchicine-binding domain. In contrast, CTR-20 fits into the colchicine site readily, nearly overlapping much of colchicine (Fig. 2d). This data suggests that the modifications of the quinolone ring are important for changing the way that the CTRs interact with the tubulin subunits in three-dimensional space. In particular, there are differences in how CTR-21 interacts with regard to hydrogen bonding and may explain why CTR-21 activity is much enhanced compared to CTR-20 and CTR-19, which contains a 7-methoxy group and arrests cells in G2/M, albeit at a much higher concentration (Supplementary Fig. S10).

The *in silico* docking may also give an indication as to why CTR-32 does not inhibit tubulin polymerization. In contrast to CTR-21, CTR-32 does not have any hydrogen bonding in the pocket. Its interactions are all hydrophobic, and the pose is different when compared to CTR-21 (Fig. 2c). The ethoxy group itself does not add any hydrogen binding potential to the compound, but does interact with β-tubulin though hydrophobic interactions. The docking suggests that CTR-32 has a different type of binding against β-tubulin than CTR-21. Nonetheless, the 2- ethoxy group on the phenyl group is important to the efficacy of the CTRs, since there is a large difference in average GI_{50} between CTR-17 and CTR-32. However, our data suggest that CTR-21 directly influences tubulin dynamics, whereas CTR-32 may not.

CTR-21 is more metabolically stable than CTR-32. Metabolic stability is another aspect of lead nomination that structural differences can affect. Therefore, we next determined the effects of the structural changes that we made in the CTRs on *in vitro* metabolism using a human microsome model of CYP450 metabolism. We found that CTR-21 is much more stable than CTR-32, with a half-life almost five times greater than the latter (Fig. 3a). This data suggests that the ethoxy group on CTR-32 is a metabolic liability (Fig. 3b). Therefore, although CTR-32 is effective at killing cancer cells, it appears that the 2-ethoxy group makes it less stable than the 2-methoxy group seen in CTR-21. Therefore, CTR-21 is the most promising agent among this series of quinolone chalcones (Fig. 3b).

CTR-21 arrests cells in G_2/M, leading to apoptosis. We anticipated that the changes made to enhance the efficacy of the CTR-21 backbone should not affect the mechanism of action since the compound could still bind to tubulin *in silico* and sought to determine if this was the case, using a combination of biochemical and cell biological approaches. We first examined the cell cycle effect of CTR-21 on HeLa and melanoma UKRV-Mel-38 cells (Fig. 4a). We found that HeLa cells arrest in G2/M by 12 hours of post-treatment with 30 nM CTR-21, and maintain the arrest even after 24 hours (Fig. 4a). We found that the majority of HeLa cells were rounded up with a short bi-polar spindle and condensed DNA by 12-hour post-CTR-21 treatment, further indication of a G2/M arrest (Fig. 4b). Finally, Western blotting data also showed that cell populations arrest in G2/M until moving into apoptotic cell death (Fig. 4c). Asynchronous HeLa cells were treated with the indicated concentration of CTR-21 and monitored over the course of 24 hours. By 6-hour post-treatment, the levels of cyclin B and cdc25 phosphorylation (i.e., indicators of G2/M arrest) increased, and peaked at 12 hours. Interestingly, the phosphorylation on the Ser62 residue of Bcl-XL is also substantially increased. By 24 hours, we see an increase of PARP cleavage, indicating that apoptosis begins to occur 24-hour post-CTR-21 treatment. Taken data together from the flow cytometry and immunofluorescence studies, CTR-21 arrests cells in G2/M, much like the previously characterized analogs CTR-20 and CTR-17. This indicates that the structural changes made to CTR-21 have not changed the underlying molecular mechanism of cell death.

CTR-21 shows synergistic effect when combined with either ABT-737 or paclitaxel. We previously showed that CTR-20 was synergistic with the Bcl-XL inhibitor ABT-737 in HeLa cells and enhanced the activity of paclitaxel in multidrug-resistant cells[10]. ABT-737 is limited in clinical use due to its severe side effect such as thrombocytopenia at the effective dose[18]. We determined if the changes we made to CTR-21 for enhancing its activity affected its ability to be synergistic with the anticancer agents. The complementary index (CI) was less than 1.0 when HeLa cells were treated with normally non-effective doses of CTR-21 (0.78 nM) in combination with low doses of ABT-737, indicating that there is clear synergism of this combination[19] (Fig. 5a). The synergistic effect was especially pronounced (CI, 0.48) where each compound alone has little effect on the survival of the cells (i.e., 1.56 μM ABT-737 and 0.78 nM CTR-21) (Fig. 5a). This data may open the possibility that the combination of these two agents can be used to treat cancers without causing side effects. We found that in MDA-MB-231TaxR cells, which are normally resistant to paclitaxel, the combinatorial effects of CTR-21 and paclitaxel showed greater synergism than the combination with ABT-737 (Fig. 5b). Even at doses where paclitaxel has little effect on the cell (18.75 nM), the addition of 23 nM of CTR-21 can synergistically enhance the cell death (CI, 0.35). These data indicate that the SAR-directed enhancements made to the CTR backbone to make the highly effective CTR-21 did not change the ability of CTRs to work synergistically with potential combinatorial partners.

Discussion

In an effort to optimize the efficacy and stability of novel quinolone chalcones CTR-17 and CTR-20, we created a small pool of derivatives with different modifications to the quinolone and/or phenyl ring moieties. We then carried out SAR analysis to determine the most effective CTR to serve as a lead in developing a highly desirable anticancer agent. We found that the most effective changes were moving the 6-methoxy group to 8-methoxy on the quinolone ring (CTR-21), and replacing the 2-methoxy with an ethoxy group (CTR-32). Both CTR-21 and CTR-32 are predicted to bind near the chalcone binding site in the α/β-tubulin dimer. This leads to the cell cycle arrest at G2/M and eventually cell death by apoptosis. However, CTR-21 has advantages over CTR-32. CTR-32 does not effectively prevent tubulin polymerization, although its binding site is almost identical to that of CTR-21. Our data also suggest that CTR-32 is much less metabolically stable. Considering this, a methoxy group is likely required for best anti-tubulin activity. Based on our SAR analysis, the position of the methoxy group on the in CTR enhances the efficacy of quinolone chalcones, since CTR-21 with an 8-methoxy on the quinolone ring is much more effective than the structural isomers CTR-19 (7-methoxy) and CTR-20 (6-methoxy). *In silico* docking comparing CTR-20 and CTR-21 suggests that CTR-21 forms two hydrogen bonds with tubulin dimers, interacting with the Pro175 of β-tubulin and Thr179 of α-tubulin residues. In contrast, CTR-20 only interacts with β-tubulin. Furthermore, CTR-21 is modeled to interact with tubulin in a unique manner, as a hybrid of chalcone and vinblastine. Thus, this simple change allows for the compound to position itself differently and as a result increases its effectiveness.

In conclusion, CTR-21 shows similar molecular properties to our previously characterized CTR-17 and CTR-20. Comparing to these two previously synthesized chalcones, however, CTR-21 is highly potent as the GI_{50} value of CTR-21 is ~ 30 times more efficient that CTR-17/CTR-20 while it is highly selective against cancer cell king (> 100 fold). We anticipate that CTR-21 has many positive characteristics to move it forward into the next stage of drug development using preclinical models.

Methods

All chemicals and solvents used were commercially available and were of reagent grade. Where measurements are listed, melting points were determined in open glass capillaries on a Veego digital melting point apparatus and were

uncorrected. The infrared (IR) spectra of compounds were recorded on Schimadzu FT-IR 8400S infrared spectrophotometer using an ATR accessory. 1H NMR spectra were recorded on a Bruker Avance II 400 spectrometer, using DMSO-d6 as solvent and tetramethylsilane (TMS) as internal standard. Mass spectral analysis was carried out using Applied Biosystem QTRAP 3200 MS/MS or Waters Xevo G2-XS Quadrupole Time-of-Flight mass spectrometer system in ESI mode. Reactions were monitored by TLC using pre-coated silica gel aluminum plates (Kieselgel 60, 254, E. Merck, Germany); zones were detected visually under ultraviolet irradiation.

General synthesis of 2 chloro-3-formyl quinolines [12] . Commercially available Acetanilide /substituted acetanilides (0.05 mol) were dissolved in 9.6 mL of dimethyl formamide (DMF, 0.125 mol), to which 32 mL of phosphorus oxychloride (0.35 mol) was added gradually at 0° C. The reaction mixture was taken in a round bottom flask (RBF) equipped with a reflux condenser fitted with a drying tube and was heated for 4–16 hours on oil bath at 75–80° C. The solution was then cooled to room temperature and subsequently poured onto 100 mL of icy water. The precipitate formed was collected by filtration and recrystallized from ethyl acetate.

General Synthesis of 2-chloroquinolinyl chalcones [13,14]. A mixture of 2-chloro-3-formyl quinolines (1 mmol), the respective acetophenones (1 mmol) and a base (either sodium methoxide (catalytic) or sodium hydroxide (one pellet)) in methanol (4 mL) was stirred at room temperature for 6–24 hours. The resulting precipitate was collected by filtration, washed with water, and recrystallized from DMF-H_2O or EtOH-H_2O.

General Synthesis of 3-(3-oxo-3-phenylprop-1-enyl)quinolin-2(1H)-ones of Formula I (Fig. 1). A suspension of the 3-(2-chloroquinolin-3-yl)-1-phenylprop-2-en-1-ones (0.001 mol) in 70% acetic acid (10 mL) was heated under reflux for 4–6 hours. Upon completion of the reaction (as indicated by a single spot in a TLC), the reaction mixture was cooled to ambient temperature and the solid product precipitated out was filtered. The filtered product was washed with water, dried and recrystallized in methanol or DMF/water.

(E)-3-(3-(2-Methoxyphenyl)-3-oxoprop-1-enyl)quinolin-2(1H)-one (CTR-17). Yield 81%; M.P. 256–258° C.; FT-IR (KBr) υ (cm^{-1}): 3153 (NH), 1656 (C□O), 1586, 1557 (C□C), 1240, 1020 (C—O—C); 1H NMR (400 MHz, DMSO-d6): (12.05 (s, 1H), 8.47 (s, 1H), 7.86 (d, J = 16.0 Hz, 1H), 7.73 (d, J = 7.9 Hz, 1H), 7.60–7.44 (m, 4H), 7.34 (d, J = 8.3 Hz, 1H), 7.26–7.19 (m, 2H), 7.08 (td, J = 7.4, 0.9 Hz, 1H), 3.87 (s, 3H); MS-API: [M + H] + 306.1 (calculated 305.1).

(E)-3-(3-(2-Methoxyphenyl)-3-oxoprop-1-enyl)-6-methylquinolin-2(1H)-one (CTR-18). Yield 86%; M.P. 222–224° C.; FT-IR (KBr) υ (cm^{-1}): 3145 (NH), 1654 (C□O), 1584, 1558 (C□C), 1241, 1019 (C—O—C); 1H NMR (400 MHz, DMSO-d6): δ 11.88 (s, 1H), 8.15 (s, 1H), 7.89 (d, J = 15.9 Hz, 1H), 7.58 (d, J = 15.9 Hz, 1H), 7.50 (t, J = 7.5 Hz, 2H), 7.44 (s, 1H), 7.32 (d, J = 8.5 Hz, 1H), 7.26 (d, J = 8.4 Hz, 1H), 7.10 (d, J = 8.3 Hz, 1H), 7.04 (t, J = 7.4 Hz, 1H), 3.90 (s, 3H), 2.39 (s, 3H), MS-API: [M + H] + 320.1 (calculated 319.12).

(E)-7-Methoxy-3-(3-(2-methoxyphenyl)-3-oxoprop-1-enyl) quinolin-2(1H)-one (CTR-19). Yield 83%; M.P. 227–229° C.; FT-IR (KBr) υ (cm^{-1}): 3144 (NH), 1656 (C□O), 1559 (C□C), 1167, 1021 (C—O—C); 1H NMR (400 MHz, DMSO-d6): δ 11.96 (s, 1H), 8.40 (s, 1H), 7.85 (d, J = 16.0 Hz, 1H), 7.60–7.42 (m, 3H), 7.32–7.18 (m, 4H), 7.08 (t, J = 7.4 Hz, 1H), 3.87 (s, 3H), 3.81 (s, 3H); MS-API: [M + H] + 336.1 (calculated 335.12).

(E)-6-Methoxy-3-(3-(2-methoxyphenyl)-3-oxoprop-1-enyl) quinolin-2(1H)-one (CTR-20). Yield 83%; M.P. 227–229° C.; FT-IR (KBr) υ (cm^{-1}); 3155 (NH), 1652 (C□O), 1597, 1558 (C□C), 1164, 1022 (C—O—C); 1H NMR (400 MHz, DMSO-d6): δ 11.91 (s, 1H), 8.37 (s, 1H), 7.78 (d, J = 15.9 Hz, 1H), 7.64 (d, J = 8.8 Hz, 1H), 7.57–7.49 (m, 2H), 7.48–7.40 (m, 1H), 7.20 (d, J = 8.5 Hz, 1H), 7.07 (t, J = 7.7 Hz, 1H), 6.89–6.81 (m, 2H), 3.85 (s, 3H), 3.84 (s, 3H); MS-API: [M + H] + 336.1 (calculated 335.12).

(E)-3-(3-(2,6-dimethoxyphenyl)-3-oxoprop-1-enyl)quinolin-2(1H)-one (CTR-25).

Yield 65%; M.P. 236–238° C.; FT-IR (ATR) υ (cm^{-1}): 3149 (NH), 1667 (C=O), 1591, 1558 (C=C), 1252, 1058 (C—O—C); 1H NMR (400 MHz, DMSO-d6): δ 12.00 (s, 1H), 8.41 (s, 1H), 7.66 (d, J = 8.0 Hz, 1H), 7.47–7.55 (m, 1H), 7.32–7.41 (m, 2H), 7.21–7.31 (m, 2H), 7.18 (t, J = 7.6 Hz, 1H), 6.73 (d, J = 8.5 Hz, 2H), 3.69 (s, 6H); MS-API: [M + H] + 336.2 (calculated 335.12).

(E)-3-(3-(2-ethoxyphenyl)-3-oxoprop-1-enyl)quinolin-2(1H)-one (CTR-32)

Yield 77%; M.P. 199–201° C.; FT-IR (ATR) υ (cm^{-1}): 3128 (NH), 1651 (C=O), 1597, 1555 (C=C), 1169, 1023 (C—O—C); 1H NMR (400 MHz, DMSO-d6): δ 12.02 (s, 1H), 8.39 (s, 1H), 8.00 (d, J = 15.8 Hz, 1H), 7.68 (dd, J = 8.0, 1.3 Hz, 1H), 7.44–7.56 (m, 4H), 7.26–7.32 (m, 1H), 7.11–7.23 (m, 2H), 7.02 (td, J = 7.5, 1.0 Hz, 1H), 4.12 (q, J = 7.0 Hz, 2H), 1.31 (t, J = 6.9 Hz, 3H). MS-API: [M + H] + 320.2 (calculated 319.12).

(E)-3-(3-(2-ethoxyphenyl)-3-oxoprop-1-enyl)-6-methoxyquinolin-2(1H)-one (CTR-40)

Yield 86%; M.P. 233–235° C.; FT-IR (KBr) υ (cm^{-1}): 3166 (NH), 1652 (C=O), 1598, 1560 (C=C), 1245, 1023 (C—O—C); 1H NMR (400 MHz, DMSO-d6): δ 11.94 (s, 1H), 8.33 (s, 1H), 8.00 (d, J = 15.8 Hz, 1H), 7.43–7.53 (m, 3H), 7.17–7.26 (m, 3H), 7.15 (d, J = 8.3 Hz, 1H), 7.02 (t, J = 7.5 Hz, 1H), 4.12 (q, J = 6.8 Hz, 2H), 3.77 (s, 3H), 1.31 (t, J = 7.0 Hz, 3H); MS-API: [M + H] + 350.2 (calculated 349.13).

(E)-8-Methoxy-3-(3-(2-methoxyphenyl)-3-oxoprop-1-enyl) quinolin-2(1H)-one (CTR-21). Yield 71%. 1H NMR (400 MHz, DMSO-d6): 3.86 (s, 3H), 3.91 (s, 3H), 7.06 (t, 1H), 7.17 (t, 3H), 7.29 (d, 1H), 7.47 (d, 1H), 7.52 (m, 2H), 7.86 (d, 1H), 8.45 (s 1H), 11.16 (1H). MS-API: [M + H] + 336.1 (Calculated: 335.12).

(E)-6,7-dimethoxy-3-(3-(2-methoxyphenyl)-3-oxoprop-1-enyl)quinolin-2(1H)-one (CTR-24)

1H NMR (400 MHz, DMSO-d6) δ 11.83 (s, 1H), 8.27 (s, 1H), 7.74 (d, J = 16.01 Hz, 1H), 7.38–7.56 (m, 3H), 7.14–7.19 (m, 2H), 7.03 (dt, J = 0.88, 7.44 Hz,1H), 6.83 (s, 1H), 3.82 (s, 3H), 3.81 (s, 3H), 3.77 (s, 3H)

(E)-3-(3-(2,5-dimethoxyphenyl)-3-oxoprop-1-enyl)quinolin-2(1H)-one (CTR-26)

1H NMR (400 MHz, DMSO-d6) δ 12.00 (s, 1H), 8.42 (s, 1H), 7.83 (d, J = 15.76 Hz, 1H), 7.69 (d, J = 8.00 Hz, 1H), 7.45–7.57 (m, 2H), 7.30 (d, J = 8.25 Hz,1H), 7.19 (t, J = 7.50 Hz, 1H), 7.04–7.14 (m, 2H), 6.98 (d, J = 2.75 Hz, 1H), 3.78 (s, 3H), 3.72 (s, 3H)

(E)-3-(3-(2,4-dimethoxyphenyl)-3-oxoprop-1-enyl)quinolin-2(1H)-one (CTR-27)

1H NMR (400 MHz, DMSO-d6) δ 11.98 (s, 1H), 8.38 (s, 1H), 7.99 (d, J = 16.01 Hz, 1H), 7.70 (d, J = 7.75 Hz, 1H), 7.49–7.58 (m, 3H), 7.30 (d, J = 8.25 Hz,1H), 7.19 (t, J = 7.50 Hz, 1H), 3.86 (s, 3H), 3.83 (s, 3H)

(E)-3-(3-(5-fluoro-2-methoxyphenyl)-3-oxoprop-1-enyl)quinolin-2(1H)-one (CTR-29)

1H NMR (400 MHz, DMSO-d6) δ 12.02 (s, 1H), 8.44 (s, 1H), 7.82 (d, J = 16.01 Hz, 1H), 7.69 (d, J = 7.75 Hz, 1H), 7.47–7.59 (m, 2H), 7.37 (dt, J = 3.25,8.63 Hz, 1H), 7.30 (d, J = 8.25 Hz, 1H), 7.26 (dd, J = 3.25, 8.76 Hz, 1H), 7.17–7.22 (m, 2H), 3.29 (s, 3H)

(E)-3-(3-(4-fluoro-2-methoxyphenyl)-3-oxo prop-1-enyl)quinolin-2(1H)-one (CTR-30)

1H NMR (400 MHz, DMSO-d6) δ 12.01 (s, 1H), 8.42 (s, 1H), 7.87 (d, J = 16.01 Hz, 1H), 7.69 (d, J = 7.75 Hz, 1H), 7.48–7.58 (m, 3H), 7.30 (d, J = 8.25 Hz,1H), 7.19 (t, J = 7.50 Hz, 1H), 7.09 (dd, J = 2.25, 11.51 Hz, 1H), 6.87 (dt, J = 2.50, 8.38 Hz, 1H), 3.86 (s, 3H)

(E)-3-(3-(2,5-dimethoxyphenyl)-3-oxoprop-1-enyl)-6-methoxyquinolin-2(1H)-one (CTR-34)

1H NMR (400 MHz, DMSO-d6) δ 11.92 (s, 1H), 8.36 (s, 1H), 7.82 (d, J = 16.01 Hz, 1H), 7.50 (d, J = 16.01 Hz, 1H), 7.18–7.26 (m, 3H), 7.07–7.12 (m, 2H), 6.98 (d, J = 2.50 Hz, 1H), 3.78 (s, 3H), 3.77 (s, 3H), 3.72 (s, 3H)

(E)-3-(3-(2,4-dimethoxyphenyl)-3-oxoprop-1-enyl)-6-methoxyquinolin-2(1H)-one (CTR-35)

1H NMR (400 MHz, DMSO-d6) δ 11.89 (s, 1H), 8.31 (s, 1H), 7.99 (d, J = 15.76 Hz, 1H), 7.57 (d, J = 2.75 Hz, 1H), 7.54 (d, J = 9.76 Hz, 1H), 7.16–7.26 (m,3H), 6.67 (d, J = 2.25 Hz, 1H), 6.62 (dd, J = 2.25, 8.51 Hz, 1H), 3.87 (s, 3H), 3.83 (s, 3H), 3.77 (s, 3H)

(E)-6-methoxy-3-(3-(2-methoxy-4-(trifluoro methoxy)phenyl)-3-oxoprop-1-enyl)quinolin-(1H)-one (CTR-36)

1H NMR (400 MHz, DMSO-d6) δ 11.94 (s, 1H), 8.37 (s, 1H), 7.83 (d, J = 15.76 Hz, 1H), 7.58 (d, J = 8.50 Hz, 1H), 7.51 (d, J = 15.76 Hz, 1H), 7.15–7.28 (m,4H), 7.04 (d, J = 8.50 Hz, 1H), 3.87 (s, 3H), 3.77 (s, 3H)

(E)-3-(3-(5-fluoro-2-methoxyphenyl)-3-oxoprop-1-enyl)-6-methoxyquinolin-2(1H)-one (CTR-37)

1H NMR (400 MHz, DMSO-d6) δ 11.94 (s, 1H), 8.37 (s, 1H), 7.82 (d, J = 16.01 Hz, 1H), 7.50 (d, J = 16.01 Hz, 1H), 7.37 (dt, J = 3.25, 8.63 Hz, 1H), 7.23–7.29 (m, 2H), 7.17–7.22 (m, 3H), 3.82 (s, 3H), 3.77 (s, 3H)

(E)-3-(3-(4-fluoro-2-methoxyphenyl)-3-oxoprop-1-enyl)-6-methoxyquinolin-2(1H)-one (CTR-38)

1H NMR (400 MHz, DMSO-d6) δ 11.91 (br. s., 1H), 8.35 (s, 1H), 7.86 (d, J = 16.01 Hz, 1H), 7.48–7.58 (m, 2H), 7.17–7.29 (m, 3H), 7.09 (dd, J = 2.50,11.51 Hz, 1H), 6.88 (dt, J = 2.38, 8.44 Hz, 1H), 3.86 (s, 3H), 3.77 (s, 3H)

Cell lines. The human MDA-MB-231, MCF7, MDA-MB-468, RPMI-8226 and HeLa cell lines were purchased from ATCC and maintained in Dulbecco's Modified Eagle Medium (DMEM) - high glucose supplemented with 10% fetal bovine serum (FBS) and antibiotics/antimycotics. Cell line authentication was carried out by Genetica DNA Laboratories (Burlington, NC) using a short tandem repeat (STR) profiling method (March 2015; July 2015; September 2016). Melanoma cells E-055 (MZ-Mel-3), E-097 (Mel-SOE), E-112 (UKRV-Mel-38), E-157 (UKRV-Mel-17) were obtained from the European Searchable Tumour Line Database (ESTDAB) cell bank (a kind gift of Dr. Graham Pawelec, Tubingen University, Germany). MDA-MB-435 was purchased from the Division of Cancer Treatment and Diagnosis Tumor Repository. All melanoma cells were cultured in Roswell Park Memorial Institute (RPMI) medium supplemented with 10% FBS and P/S/antimycotics. Primary human epidermal melanocytes from normal adult abdominal skin were purchased from ATCC (cat # PCS-200-013) and Cell Applications (cat#104-05a). The melanocytes were cultured in the media supplied by the companies.

Sulforhodamine B (SRB) assay. The SRB assay was used to assess drug-induced cytotoxicity and cell proliferation as previously described[20–22] with a few modifications. Briefly, cells were plated 10,000 to 25,000 cells/cm^2 in 96-well plates (100 µl medium) and allowed to adhere overnight. The cell counts were different for each cell line to ensure optimal cell growth for the duration of the assay. Eight different concentrations of compound solutions using 2–4 times serial dilutions (100 µl). Cells were then incubated for an additional 48 hours and then fixed with 100 µl ice-cold 10% (w/v) trichloroacetic acid (TCA) (without removing the cell medium, final concentration, 3.3% of TCA)

and stained with 0.4% SRB (w/v) in 1% acetic acid (v/v). The relative growth rate (%) was calculated for each of the compound concentrations according to the following formula: 100 * (T – T0)/(C – T0), in which T is the optical density (OD) after exposure to a certain concentration of the compound after 48 hours, T0 is the OD at the start of drug exposure (time zero) and C is the control growth. The GI_{50} for each compound was obtained from a non-linear sigmoidal dose-response (variable slope) curve fitted by GraphPad Prism v.4.03 software.

PBMCs isolation. Peripheral blood mononuclear cells from healthy donors were isolated by density gradient centrifugation using Ficoll solution. Briefly, whole blood (collected from Canadian Blood Services under Institutional Research Ethics Board Project # 18–099) was gently layered over an equal volume of Ficoll and centrifuged at 800 ×*g* for 20 minutes with no brake. The Buffy coat was carefully collected by pipetting in 50 mL tubes and topped off with PBS. The cell isolates were subsequently mixed by inversion and centrifuged at 300 ×*g* for 12 minutes. The supernatant was then carefully aspirated without disturbing the cell pellet, and the PBMCs were resuspended in ammonium-chloride-potassium (ACK) lysis buffer. The tubes were left to stand for 15 minutes to allow for red blood cell lysis. PBS was again added to the cells and centrifuged at 300 ×*g* for 12 minutes and pelleted PBMCs were resuspended in RPMI + 10% heat inactivated FBS. Following counting, cells were centrifuged again and cryopreserved with a freezing medium composed of 40% FBS, 10% DMSO and 50% culture medium. Cryovials were placed in a − 80°C for 24 hours prior to transfer to liquid nitrogen for long-term storage.

PBMCs thawing. PBMC cryovials were transferred from liquid nitrogen and placed in a 37°C water bath until almost completely thawed. 1 mL of pre-warmed medium was added drop-wise and the entire contents of the cryovial was transferred to a 15-mL tube. Pre-warmed medium was then added to bring the volume up to 10 mL. The PBMCs were centrifuged at 300 ×*g* for 10 minutes, and the cell pellet was gently resuspended with 5 mL of warm medium. The tubes were subsequently placed in a 37°C incubator in a 5° angled rack for 4 hours. An additional 5 mL warm medium containing of 30 units/mL benzonase nuclease was then injected into the cell solution and left to stand at room temperature for 5 minutes before centrifugation for 10 minutes at 300 ×*g*. The pelleted cells were resuspended in the medium with 100 units/mL of IL-2 (Cedarlane Laboratories, Burlington, ON, Canada) and a small aliquot was used for cell counting and viability staining. The cells were plated in 96-well plates at a density of 80,000-120,000 cellules/well/100 µL.

PBMCs culture and MTS assay. Following a 48-hour incubation period, eight different concentrations of compound solutions using two to four-fold serial dilutions were added to the cells (100 µl). Cells were incubated for an additional 48 hours and cytotoxicity was established using the CellTiter 96 cytotoxicity assay (Promega). 40 µl of the tetrazolium dye was added to each well of the plate and then incubated for 2 hours. OD was then read directly at 490 nm using the automated Biotek Synergy H4 plate reader. The GI_{50} was calculated similarly to the SRB.

Cell cycle analysis by flow cytometry. Cell cycle progression was determined using flow cytometry. UKRV-Mel-38 and HeLa cells were plated onto 10 cm plate at a density of 0.5 million and treated them with or without the compounds the following day for 12, 24 or 48 hours. Cells were then harvested and centrifuged at 1,000 rpm for 5 minutes, washed in PBS and then fixed with ice-cold ethanol (70%) for at least 24 hours at − 20°C. The cells were centrifuged, re-suspended in PBS solution, followed by centrifugation. The cell pellet was then stained with 100 µg/mL propidium iodide (PI) and 100 µg/mL RNase A in distilled water for at least 1 hour. DNA content was measured using a Beckmann Coulter Cytomics FC500 (Beckman Coulter, Fullerton, CA), and the proportion of cell populations in G0/G1, S, and G2/M phases of cell cycle was calculated on the basis of DNA distribution histograms using CXP software (Beckman Coulter, Fullerton, CA)

Cell Cycle Analysis by immunofluorescence and Western blots. Cell cycle analysis, including immunofluorescence and western blot analysis was carried out as described previously[10].

Tubulin polymerization assay. Microtubule assembly was assessed using a Tubulin Polymerization assay kit (BK011P; Cytoskeleton Inc., Denver, CO). Purified porcine tubulin proteins (> 99% purity) were suspended in G-PEM buffer containing 80 mM PIPES, 2 mM MgCl2, 0.5 mM EGTA, 1 mM GTP (pH 6.9) and 20% glycerol. Polymerization was started by incubating at 37°C and followed by absorbance readings every 1 minute at 340 nm for 1 hour using a Synergy H4 plate reader.

Microsome-based assay. Microsome metabolism assay was carried out as per manufacturer protocol (ThermoFisher), with 5 µM of starting compound. Analytes were measured on a Waters Xevo G2-XS Quadrupole Time-of-Flight mass spectrometer. Half-life was calculated using exponential one phase decay (GraphPad Prism 5). Hydroxychloroquine was used as an internal standard (500 pg/µL).

Declarations

Competing Interests

The authors declare that they have no competing interests.

AUTHOR CONTRIBUTIONS

J.K. and A.D carried out experiments and drafted initial manuscript; I.K.L. carried out experiments; C.K. synthesized chemicals; P.T. guided the synthesis of chemicals; and H.L. led the entire study and wrote the final version of manuscript. All authors reviewed the manuscript.

Acknowledgements

The authors are grateful to Dr. Graham Pawelec, a Professor at Tubingen University for the panel of 82 melanoma cell line collection. HL is grateful to the funders for this work: The Natural Sciences and Engineering Research Council of Canada (NSERC), Northern Ontario Heritage Funds Corporation, Northern Cancer Foundation, and Canadian Institute of Health Research (CIHR).

References

1 Bates, D. & Eastman, A. Microtubule destabilising agents: far more than just antimitotic anticancer drugs. *British journal of clinical pharmacology* **83**, 255-268, doi:10.1111/bcp.13126 (2017).

2 Field, J. J., Kanakkanthara, A. & Miller, J. H. Microtubule-targeting agents are clinically successful due to both mitotic and interphase impairment of microtubule function. *Bioorganic & medicinal chemistry* **22**, 5050-5059, doi:10.1016/j.bmc.2014.02.035 (2014).

3 Jordan, M. A. & Wilson, L. Microtubules as a target for anticancer drugs. *Nature reviews. Cancer* **4**, 253-265, doi:10.1038/nrc1317 (2004).

4 Dumontet, C. & Jordan, M. A. Microtubule-binding agents: a dynamic field of cancer therapeutics. *Nature reviews. Drug discovery* **9**, 790-803, doi:10.1038/nrd3253 (2010).

5 Lu, Y., Chen, J., Xiao, M., Li, W. & Miller, D. D. An overview of tubulin inhibitors that interact with the colchicine binding site. *Pharmaceutical research* **29**, 2943-2971, doi:10.1007/s11095-012-0828-z (2012).

6 Schmidt, M. & Bastians, H. Mitotic drug targets and the development of novel anti-mitotic anticancer drugs. *Drug resistance updates : reviews and commentaries in antimicrobial and anticancer chemotherapy* **10**, 162-181, doi:10.1016/j.drup.2007.06.003 (2007).

7 Stanton, R. A., Gernert, K. M., Nettles, J. H. & Aneja, R. Drugs that target dynamic microtubules: a new molecular perspective. *Medicinal research reviews* **31**, 443-481, doi:10.1002/med.20242 (2011).

8 Ducki, S. *et al.* Potent antimitotic and cell growth inhibitory properties of substituted chalcones. *Bioorganic & medicinal chemistry letters* **8**, 1051-1056, doi:10.1016/s0960-894x(98)00162-0 (1998).

9 Li, L. *et al.* Recent advances in trimethoxyphenyl (TMP) based tubulin inhibitors targeting the colchicine binding site. *European journal of medicinal chemistry* **151**, 482-494, doi:10.1016/j.ejmech.2018.04.011 (2018).

10 Lindamulage, I. K. *et al.* Novel quinolone chalcones targeting colchicine-binding pocket kill multidrug-resistant cancer cells by inhibiting tubulin activity and MRP1 function. *Scientific reports* **7**, 10298, doi:10.1038/s41598-017-10972-0 (2017).

11 Vogel, A. I., Tatchell, A.R., Furnis, B.S., Hannaford, A.J, and Smith, P.W.G. *Vogel's Textbook of Practical Organic Chemistry*. (Prentice Hall, 1996).

12 Meth-Cohn, O., Narine, B. & Tarnowski, B. A versatile new synthesis of quinolines and related fused pyridines. Part 7. The conversion of acetamidothiophens into thienopyridines. *Journal of the Chemical Society, Perkin Transactions 1*, 1531-1536, doi:10.1039/P19810001531 (1981).

13 Dominguez, J. N. *et al.* Synthesis of quinolinyl chalcones and evaluation of their antimalarial activity. *European journal of medicinal chemistry* **36**, 555-560, doi:10.1016/s0223-5234(01)01245-4 (2001).

14 Li, R. *et al.* In vitro antimalarial activity of chalcones and their derivatives. *Journal of medicinal chemistry* **38**, 5031-5037, doi:10.1021/jm00026a010 (1995).

15 Abonia, R. *et al.* Synthesis of novel quinoline-2-one based chalcones of potential anti-tumor activity. *European journal of medicinal chemistry* **57**, 29-40, doi:10.1016/j.ejmech.2012.08.039 (2012).

16 Lee, H., Trivedi, P., Karthikeyan, C, Lindamulage, I.K. Quinolone chalcone compounds and uses thereof. Canada patent (2017).

17 Venghateri, J. B., Gupta, T. K., Verma, P. J., Kunwar, A. & Panda, D. Ansamitocin P3 depolymerizes microtubules and induces apoptosis by binding to tubulin at the vinblastine site. *PloS one* **8**, e75182, doi:10.1371/journal.pone.0075182 (2013).

18 Zhang, H. *et al.* Bcl-2 family proteins are essential for platelet survival. *Cell death and differentiation* **14**, 943-951, doi:10.1038/sj.cdd.4402081 (2007).

19 Chou, T. C. Theoretical basis, experimental design, and computerized simulation of synergism and antagonism in drug combination studies. *Pharmacological reviews* **58**, 621-681, doi:10.1124/pr.58.3.10 (2006).

20 Solomon, V. R., Pundir, S. & Lee, H. Examination of novel 4-aminoquinoline derivatives designed and synthesized by a hybrid pharmacophore approach to enhance their anticancer activities. *Scientific reports* **9**, 6315, doi:10.1038/s41598-019-42816-4 (2019).

21 Vichai, V. & Kirtikara, K. Sulforhodamine B colorimetric assay for cytotoxicity screening. *Nature protocols* **1**, 1112-1116, doi:10.1038/nprot.2006.179 (2006).

22 Voigt, W. Sulforhodamine B assay and chemosensitivity. *Methods in molecular medicine* **110**, 39-48, doi:10.1385/1-59259-869-2:039 (2005).

Figures

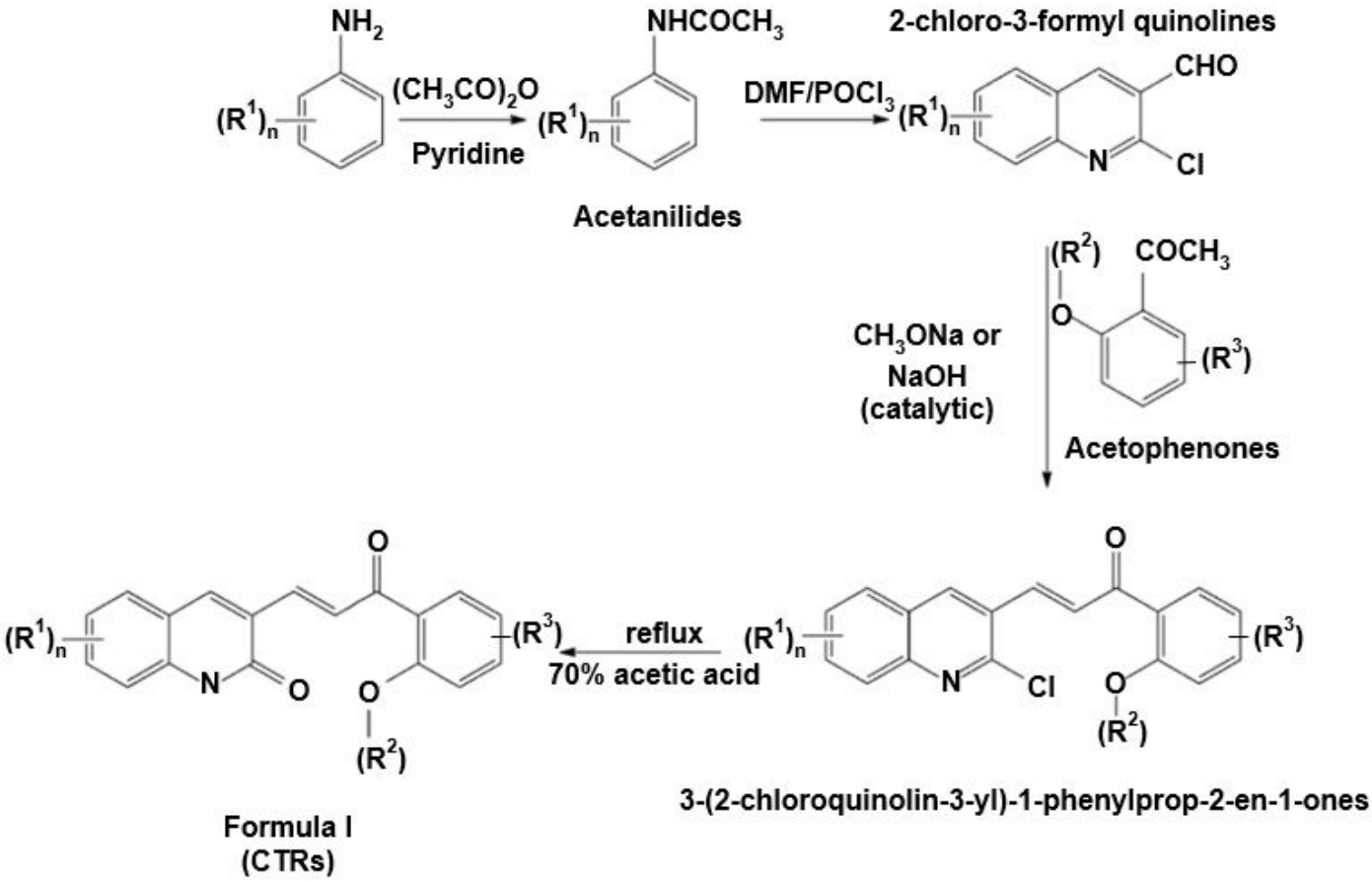

CTRs	R1	R2	R3	CTRs	R1	R2	R3
CTR-17	H	methyl	H	CTR-30	H	methyl	4-fluoro
CTR-18	6-methyl	methyl	H	CTR-32	H	ethyl	H
CTR-19	7-methoxy	methyl	H	CTR-33	6-methyl	methyl	6-methoxy
CTR-20	6-methoxy	methyl	H	CTR-34	6-methoxy	methyl	5-methoxy
CTR-21	8-methoxy	methyl	H	CTR-35	6-methoxy	methyl	4-dimethoxy
CTR-24	6,7-dimethoxy	methyl	H	CTR-36	6-methoxy	methyl	4-trifluoromethoxy
CTR-25	H	methyl	6-methoxy	CTR-37	6-methoxy	methyl	5-fluoro
CTR-26	H	methyl	5-methoxy	CTR-38	6-methoxy	methyl	4-fluoro
CTR-27	H	methyl	4-methoxy	CTR-40	6-methoxy	methyl	H
CTR-29	H	methyl	5-fluoro				

Figure 1

Synthesis Scheme and Structures for quinolone chalcones analogs.

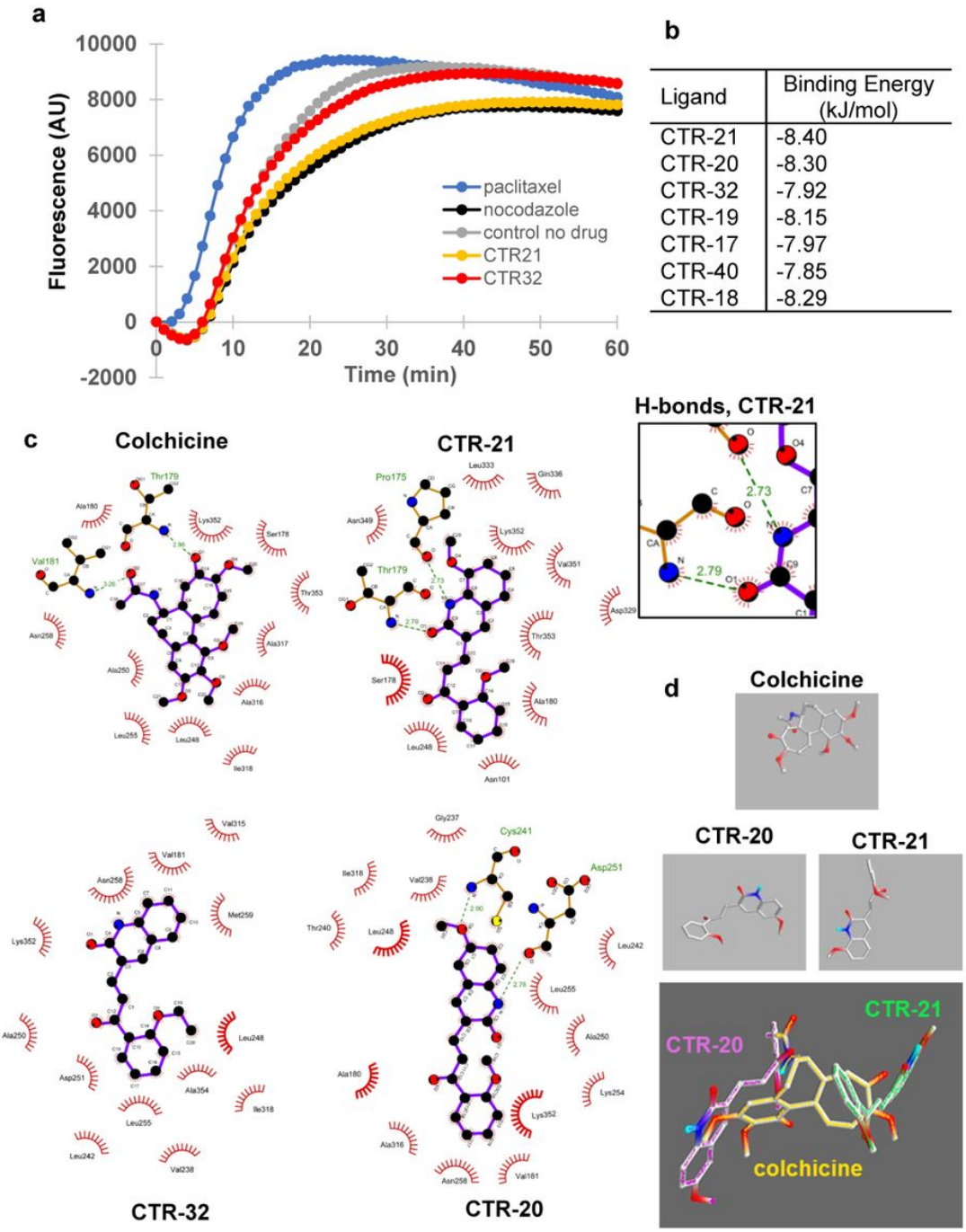

Figure 2

CTR-21 inhibits microtubule polymerization through its binding to the pocket located at the colchicine- and vinblastine-binding pockets in β-tubulin. (a) CTR-21 inhibits microtubule polymerization in vitro. Spontaneous polymerization of porcine tubulin was initiated with the addition of 1 mmol/L GTP at 37 °C and monitored every minute for 60 minutes in the presence of 3 μmol/L of CTR-21, CTR-32, nocodazole, paclitaxel, or a DMSO vehicle control. (b) CTRs dock with similar energies with alpha/beta tubulin. Shown are the best binding energies of CTRs in the interface between alpha and beta tubulin (PDB:4O2B). (c) CTR-21 is predicted to form hydrogen bonds with both

α- and β-tubulin overlapping the colchicine-binding site. Two-dimensional representations of colchicine, CTR-20, CTR-21 and CTR-32 bound to interface between alpha and beta tubulin (PDB:4O2B) according to data obtained using the LigPlot+ software. Green lines indicate hydrogen bonds (with bond length in Ångstrom), red hemi-circles depict hydrophobic interactions. The color codes are as follows: oxygen, red; nitrogen, blue; sulfur, yellow; and carbon, black. The box is the enlarged portion of CTR-21 that forms hydrogen bonds with tubulin residues. (d) CTR-21 binds perpendicularly to colchicine. Three-dimensional representation of CTR-20 and CTR-21 bound in lowest energy poses from (b), in comparison with colchicine. Color codes are: oxygen, red; nitrogen, blue; and carbon, grey. In the bottom panel, the color codes of compound names and those of compound structures are the same.

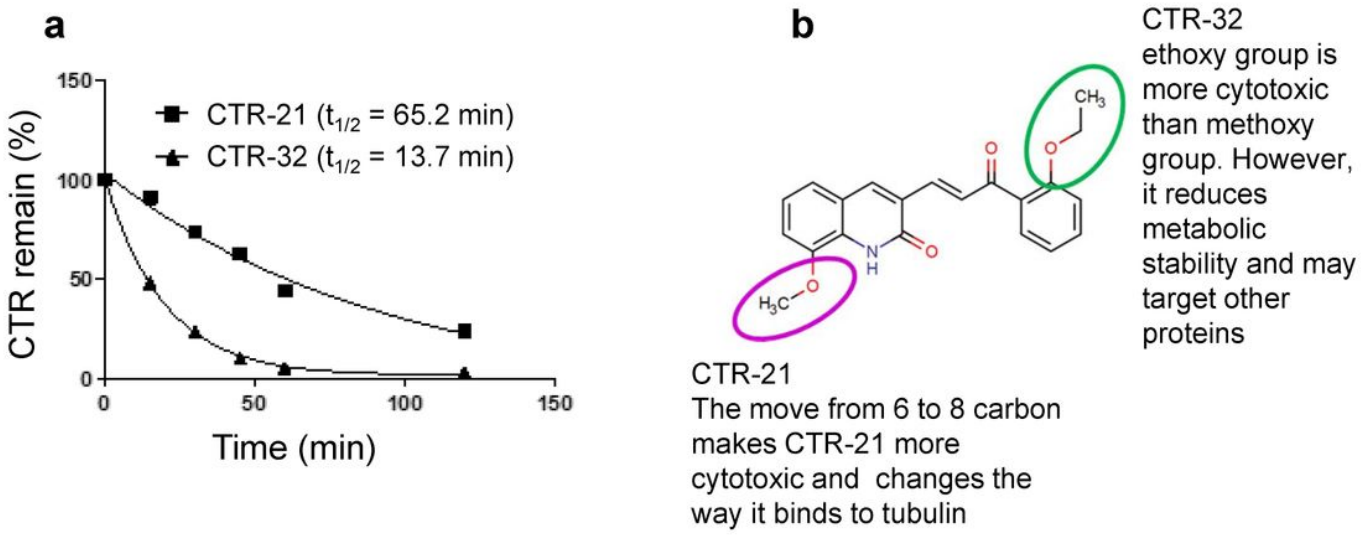

Figure 3

CTR-21 is the most active and stable one among this series. (a) CTR-21 is much more metabolically stable than CTR-32. 5 μM of CTR-21 or CTR-32 were incubated with human microsomes (20 mg/ml protein) in the presence of NADPH over the course of 120 minutes. The lysates were analyzed and % remaining CTR compounds were identified and estimated using HPLC-MS. (b) Summary of structure-activity relationship (SAR) based on activity and metabolic stability.

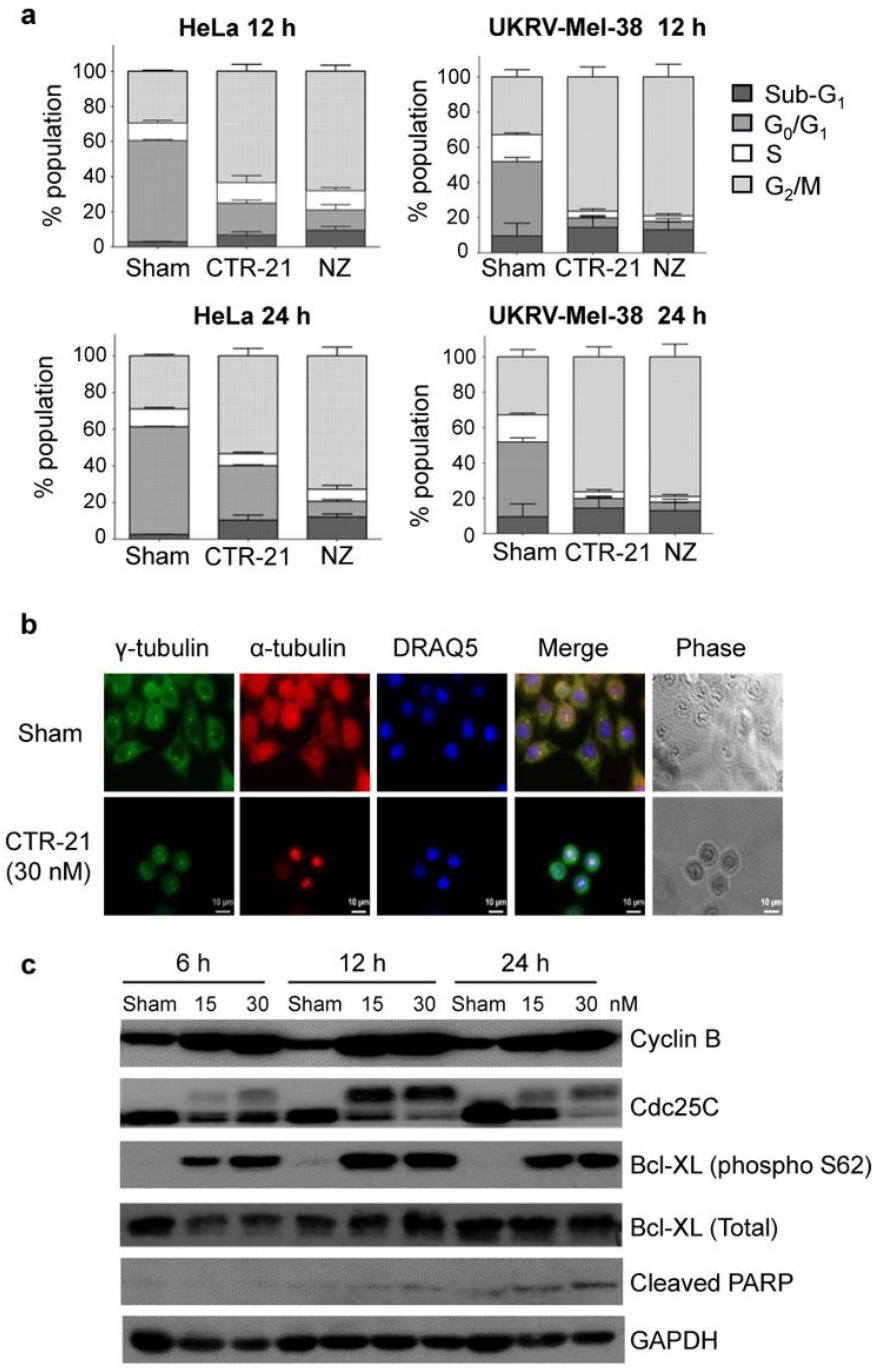

Figure 4

CTR-21 arrests cells at G2/M, leading to cell death by apoptosis. (a) Effects of CTR-21 on the cell cycle progression of HeLa and E112 cells. Cells were treated with three times of GI50 concentrations of CTR-21 or nocodazole for 12 hours and 24 hours, stained with propidium iodide (PI), and then analysed cell cycle positions using flow cytometry. (b) Cell morphology of CTR-21 arrested cells. HeLa cells were treated with 30 nM of CTR-21 for 12 hours, fixed with methanol and immunostained with α-tubulin or γ-tubulin, and counterstained with DAPI. Bar=10 μM. (c) CTR-21 promotes PARP cleavage. Data from Western blotting with whole cell extracts of asynchronously growing population show that CTR-21 causes apoptosis, which is manifested by PARP cleavage. GAPDH was used as a loading control.

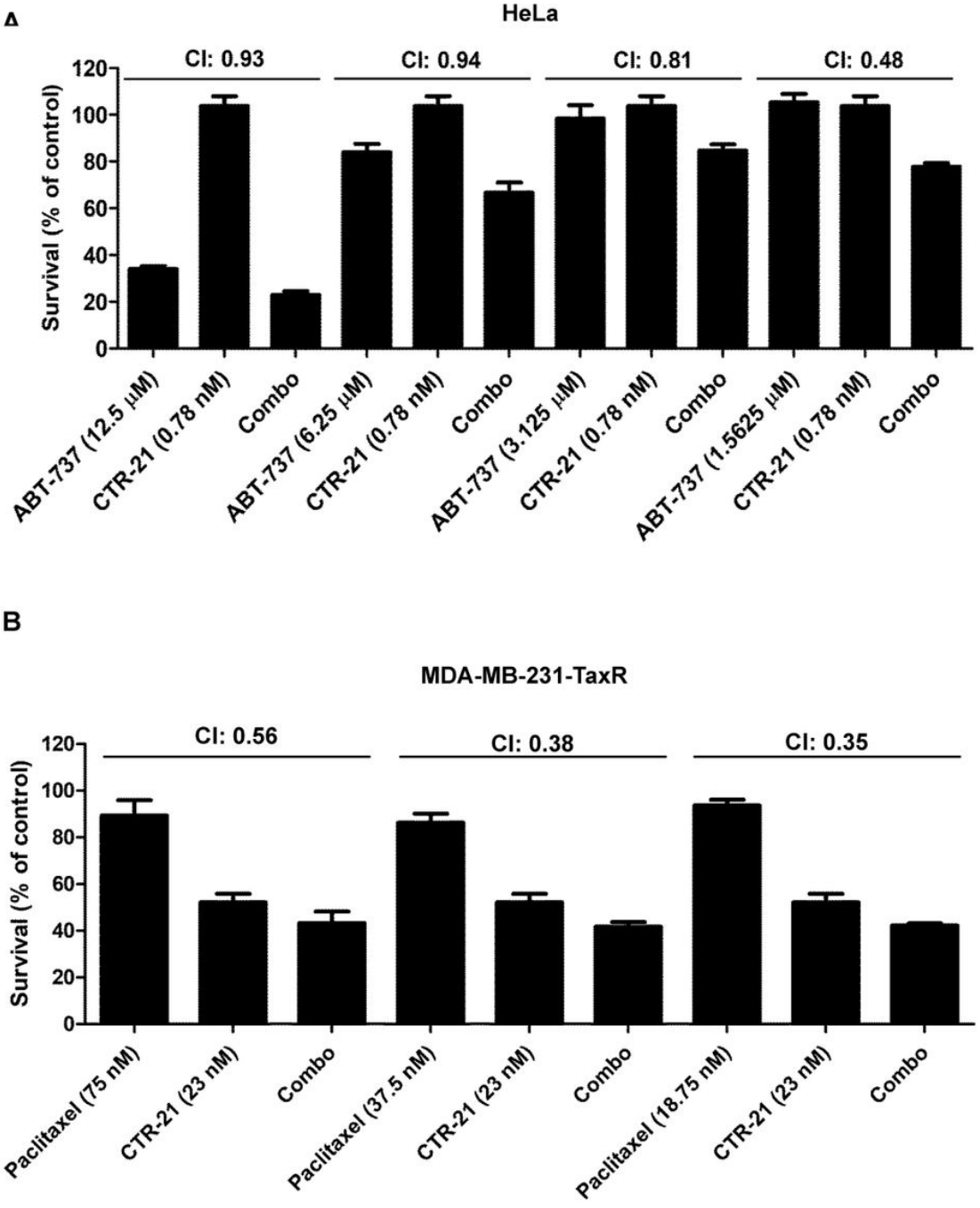

Figure 5

CTR-21 shows strong synergistic effects when combined with ABT-737 (Bcl-XL inhibitor) or paclitaxel. (a) CTR-21 kills HeLa in a synergistic manner with ABT-737. Cells were treated with 0.78 nM CTR-21 and indicated concentrations of ABT-737. CI denotes combinatorial index, calculated according to described previously19. (b) CTR-21 effectively kills paclitaxel-resistant cells when combined with paclitaxel. MDA-MB-231TaxR cells were treated with 23 nM of CTR-21 and indicated concentrations of paclitaxel.

Supplementary Files

This is a list of supplementary files associated with this preprint. Click to download.

- KnocklebySupplementalInformationR.pdf